INTERNATIONAL JOURNAL FOR NUMERICAL METHODS IN FLUIDS
Int. J. Numer. Meth. Fluids 2007; **53**:1049–1062
Published online 20 September 2006 in Wiley InterScience (www.interscience.wiley.com). DOI: 10.1002/fld.1358

Comparing analytical and numerical solution of nonlinear two and three-dimensional hydrostatic flows

Vincenzo Casulli*,† and Paola Zanolli

University of Trento, 38050 Povo (Trento), Italy

SUMMARY

New test cases for frictionless, three-dimensional hydrostatic flows have been derived from some known analytical solutions of the two-dimensional shallow water equations. The flow domain is a paraboloid of revolution and the flow is determined by the initial conditions, the nonlinear advective terms, the Coriolis acceleration and by the hydrostatic pressure. Wetting and drying is also included.

Some specific properties of the exact solutions are discussed under different hypothesis and relative importance of the forcing terms. These solutions are proposed for testing the stability, the accuracy and the efficiency of numerical models to be used for simulating environmental hydrostatic flows.

The computed solutions obtained with a semi-implicit finite difference—finite volume algorithm on unstructured grid are compared with the corresponding analytical solutions in both two and three space dimension. Excellent agreement are obtained for the velocity and for the resulting water surface elevation. Comparison of the computed inundation area also shows a good agreement with the analytical solution with degrading accuracy observed when the inundation area becomes relatively large and for long simulation time.

Received 15 February 2006; Revised 17 July 2006; Accepted 30 July 2006

KEY WORDS: shallow water; test cases; hydrostatic flows; analytical solutions; semi-implicit methods; free-surface

1. INTRODUCTION

In recent years numerical modelling of free-surface hydrodynamics has been successfully addressed by means of two and three-dimensional numerical methods that are routinely used for the numerical simulations of hydrostatic flows in environmental problems. Several different numerical methods have been developed, tested and applied during the last three decades. These range from finite differences (see, e.g. References [1, 2]), finite elements (see, e.g. References [3–6]) to finite volume

*Correspondence to: Vincenzo Casulli, University of Trento, 38050 Povo (Trento), Italy.
†E-mail: vincenzo.casulli@unitn.it

methods (see, e.g. References [7–9]). The time discretization adopted can be explicit [10], mode splitting [11, 12], or semi-implicit [1–9, 13–15].

For large-scale hydrostatic flows, the relevant forcing terms are advection, pressure and Coriolis acceleration. The wetting and drying process is often of major importance in, e.g. storm surge simulations where the location of a moving shoreline is used to predict the extent of an inundation.

A newly developed numerical algorithm is always tested against the solution of known flow problems and verified with measurements. Comparisons of the computed results with analytical solutions are also carried out in a few particular cases such as those arising from the linear shallow water theory (see, e.g. Reference [7]). Verifications and validations of numerical models for two and three-dimensional shallow water models is an endless process because of a large variety of complex phenomena that are not all present at the same time in each specific application.

In a paper published by Thacker [16], some exact solutions to the nonlinear, two-dimensional shallow water equations were provided where advection, pressure and Coriolis acceleration could all be given a relatively high importance by an appropriate choice of the free parameters. In all cases a moving shoreline was determined as part of the solution.

Numerical treatment of nonlinear advection, pressure and Coriolis terms is often uneasy when stability, accuracy and efficiency are sought. Accurate simulation of wetting and drying is even more difficult especially when the inundation area is relatively large (see, e.g. References [12, 17–19]).

In this paper, the analytical solutions presented by Thacker [16] are reconsidered and extended to three-dimensional hydrostatic flow problems where the vertical component of the velocity, though small, may have a crucial role. These analytical solutions are proposed as a standard against which the results of three-dimensional numerical models could be compared.

A recently developed semi-implicit finite difference—finite volume method (see Reference [7]) is then considered and applied. The resulting numerical solutions for the two and three-dimensional test cases are compared with the corresponding analytical solutions. Excellent agreements are obtained for the velocity components and for the resulting water surface elevation. Comparison of the computed inundation area also shows a good agreement with the analytical solution with degrading accuracy when the inundation area becomes relatively large.

In Section 2 the governing two-dimensional equations for inviscid shallow flows are derived from the more general three-dimensional hydrostatic equations to show that any solution of the two-dimensional equations also satisfy the corresponding three-dimensional counterpart and the resulting vertical component of the velocity is a linear function of the vertical coordinate. In Section 3 a two-dimensional numerical model is applied and the corresponding numerical results are compared with the known analytical solution. In Section 4 the three-dimensional extension of this numerical model is applied and the resulting numerical solution is compared with the three-dimensional analytical counterpart. The paper is concluded with a discussion on the relative importance of the accuracy of a given numerical model and the validity of governing equations.

2. TWO AND THREE-DIMENSIONAL SHALLOW WATER EQUATIONS

The governing three-dimensional equations are the Reynolds averaged Navier–Stokes equations that express the physical principle of conservation of momentum and water volume. Under the assumption that the flow is inviscid and hydrostatic, these equations (see, e.g. Reference [7]) are:

$$u_t + uu_x + vu_y + wu_z + g\eta_x - fv = 0 \tag{1}$$

DOI: 10.1002/fld

$$v_t + uv_x + vv_y + wv_z + g\eta_y + fu = 0 \tag{2}$$

$$u_x + v_y + w_z = 0 \tag{3}$$

where $u(x, y, z, t)$, $v(x, y, z, t)$ and $w(x, y, z, t)$ are the velocity components in the horizontal x, y and vertical z-directions, respectively; g is the gravity acceleration; $\eta(x, y, t)$ is the free-surface elevation and f is the Coriolis parameter.

Assuming bottom impermeability, the normal component of the velocity at the sea bed must vanish. This is expressed by the following kinematic condition:

$$uh_x + vh_y + w = 0 \quad \text{at } z = -h \tag{4}$$

where $h(x, y)$ is the bathymetry measured from the undisturbed water surface.

The kinematic condition at the free-surface is given by

$$\eta_t + u\eta_x + v\eta_y = w \quad \text{at } z = \eta \tag{5}$$

The two-dimensional shallow water equations are derived by integrating Equations (1)–(3) over depth. Thus, after using the boundary conditions (4)–(5), one gets

$$(HU)_t + (HUU)_x + (HUV)_y + gH\eta_x - fHV + R_1 = 0 \tag{6}$$

$$(HV)_t + (HUV)_x + (HVV)_y + gH\eta_y + fHU + R_2 = 0 \tag{7}$$

$$\eta_t + (HU)_x + (HV)_y = 0 \tag{8}$$

where $H(x, y, t) = h(x, y) + \eta(x, y, t)$ is the total water depth; $U(x, y, t) = (1/H)\int_{-h}^{\eta} u\,\mathrm{d}z$ and $V(x, y, t) = (1/H)\int_{-h}^{\eta} v\,\mathrm{d}z$ are the vertically averaged horizontal velocities and

$$R_1 = \left[\int_{-h}^{\eta} (u - U)^2\,\mathrm{d}z\right]_x + \left[\int_{-h}^{\eta} (u - U)(v - V)\,\mathrm{d}z\right]_y \tag{9}$$

$$R_2 = \left[\int_{-h}^{\eta} (u - U)(v - V)\,\mathrm{d}z\right]_x + \left[\int_{-h}^{\eta} (v - V)^2\,\mathrm{d}z\right]_y \tag{10}$$

The two dimensional, vertically integrated shallow water equations for frictionless flows are obtained from (6)–(8) after standard approximations of local velocities with their vertical average, so that R_1 and R_2 are neglected and the two-dimensional shallow water equations are assumed to be

$$U_t + UU_x + VU_y + g\eta_x - fV = 0 \tag{11}$$

$$V_t + UV_x + VV_y + g\eta_y + fU = 0 \tag{12}$$

$$\eta_t + (HU)_x + (HV)_y = 0 \tag{13}$$

The set of Equations (1)–(5) and (11)–(13) for the three and two-dimensional shallow water flow, respectively, are quite difficult to solve numerically because the stabilizing terms arising from viscosity and bottom friction have been neglected.

DOI: 10.1002/fld

It is worth noting that if u, v, w and η are exact solutions of the three-dimensional equations (1)–(5) and u and v are *independent* from the vertical coordinate z, then the vertical component of the velocity can be derived from Equations (3) and (4) and is given by

$$\begin{aligned} w &= w(-h) - \int_{-h}^{z} (u_x + v_y)\,\mathrm{d}\xi \\ &= -uh_x - vh_y - (u_x + v_y)(z + h) \end{aligned} \tag{14}$$

In this case, Equations (9)–(10) imply $R_1 = R_2 = 0$, thus $U = u$, $V = v$ and η are also exact solutions of the two-dimensional equations (11)–(13).

Vice versa, if U, V and η are exact solutions of the two-dimensional equations (11)–(13), then $u = U$, $v = V$ and η are also exact solutions of the three-dimensional equations (1)–(5) with w given by Equation (14).

In general, however, R_1 and R_2 are nonzero. This is typically the case when vertical viscosity, bottom friction and wind shear are considered. In this case the two-dimensional shallow water Equations (11)–(13) include an approximation that results from the assumption $R_1 = R_2 = 0$.

3. TWO-DIMENSIONAL FLOW WITH PLANAR FREE-SURFACE

The two and three-dimensional flows to be considered take place in a basin described by a paraboloid of revolution given by

$$h = h_0 \left(1 - \frac{x^2 + y^2}{L^2}\right) \tag{15}$$

where h_0 and L are positive constants. The equilibrium shoreline, determined by the condition $h = 0$, is a circle of radius L.

In such a basin, assuming a periodic flow with planar free-surface, Thacker [16] derived two basic, nontrivial solutions given by

$$U = -\psi\omega \sin \omega t \tag{16}$$

$$V = \pm\, \psi\omega \cos \omega t \tag{17}$$

$$\eta = \psi \frac{h_0}{L^2}(2x \cos \omega t \pm 2y \sin \omega t - \psi) \tag{18}$$

where the constant ψ determines the amplitude of the motion and ω is the frequency. For a specified frequency ω, with $\omega > |f|$, the radius of the equilibrium shoreline is given by

$$L = \sqrt{\frac{2gh_0}{\omega(\omega \pm f)}} \tag{19}$$

From Equation (18) it is clear that the free-surface is a linear function of x and y at all times. Moreover, from Equations (15) and (18), at every time, the moving shoreline is a circle satisfying the equation $H = h + \eta = 0$, that is,

$$(x - \psi \cos \omega t)^2 + (y \mp \psi \sin \omega t)^2 = L^2 \tag{20}$$

DOI: 10.1002/fld

hence the motion is such that the centre of the circle orbits the centre of the basin. The wet area is then a constant $A_{\text{wet}} = \pi L^2$ and the total area where the flow takes place is $A_{\text{tot}} = \pi(L + \psi)^2$.

Although the analytical solution (16)–(18) is defined and satisfies the shallow water Equations (11)–(13) over the entire (x, y) plane, these equations are of hyperbolic type only in the region where $H > 0$, that is, inside the circle defined by Equation (20). Moreover, the subcritical flow regime ($U^2 + V^2 < gH$) is confined inside the inner circle given by

$$(x - \psi \cos \omega t)^2 + (y \mp \psi \sin \omega t)^2 = L^2 \left(1 - \frac{\psi^2 \omega^2}{g h_0}\right) \tag{21}$$

and it is supercritical elsewhere. Of course, if $\psi^2 \omega^2 > g h_0$ the flow is everywhere supercritical.

The analytical solution (16)–(18), though relatively simple, represents a severe test case for most two dimensional methods (see, e.g. Reference [19]). One major difficulty arises from the absence of bottom friction and horizontal viscosity. In fact, when properly discretized, these terms have a stabilizing effect on the corresponding numerical solution. Another major difficulty is the correct determination of the wet region with acceptable accuracy.

The free parameters h_0, f, ω and ψ can be chosen in a variety of ways to give different emphasis to the forcing terms. Moreover, since U and V are independent of x and y, this solution also satisfies the linearized shallow water equations obtained from (11)–(13) by neglecting the horizontal advective terms:

$$U_t + g\eta_x - fV = 0 \tag{22}$$

$$V_t + g\eta_y + fU = 0 \tag{23}$$

$$\eta_t + (HU)_x + (HV)_y = 0 \tag{24}$$

Thus, for example, to test a numerical scheme for the pressure terms, one can assume $f = 0$ and attempt to approximate (16)–(18) by solving the simplified Equations (22)–(24). Next, if the nonlinear advective terms are included into the numerical method, one can explore possible inaccuracy introduced by the advective scheme. Finally, the above tests can be completed by using a nonzero Coriolis parameter.

For illustrative purpose, the three-dimensional numerical model described in Reference [7] will be considered by specifying only one vertical layer in order to solve the two-dimensional shallow water Equations (22)–(24). This is an efficient semi-implicit finite difference-finite volume algorithm that uses unstructured orthogonal grids (see Reference [7] for details).

As an example, some realistic values corresponding to a typical environmental flow will be considered. Thus, by setting $h_0 = 50\,\text{m}$, a latitude of 45°North and $\omega = 2\pi/(12 \times 3600)$, the resulting wave period is $T = 12\,\text{h}$ and, from Equation (15), one has $L = 164.69\,\text{km}$. Moreover, $\psi = L/10$ is chosen.

Since the chosen grid may have a significant influence on the resulting numerical accuracy, in generating an unstructured model grid it is always recommended to properly account for the given bottom topography and for the expected flow field in order to reduce the discretization error (see, e.g. References [7, 8]). With this objective, an unstructured orthogonal grid is constructed by taking mixed, triangular and quadrilateral polygons in such a fashion that their vertices all lie on concentric circles equally spaced at a distance $\Delta R = (L + \psi)/N$ and such that their sides never exceed ΔR (see Figure 1). By choosing $N = 220$, the resulting grid contains $N_p = 295\,061$ polygons and $N_s = 588\,080$ sides.

DOI: 10.1002/fld

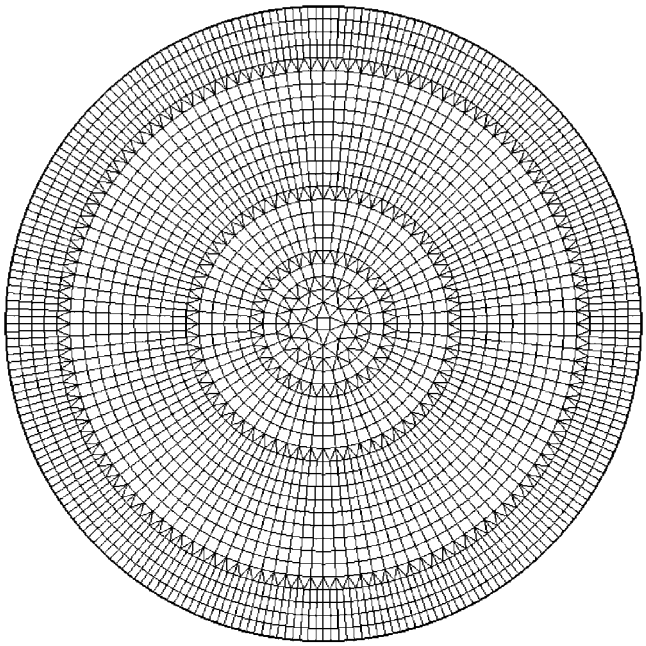

Figure 1. Unstructured orthogonal grid.

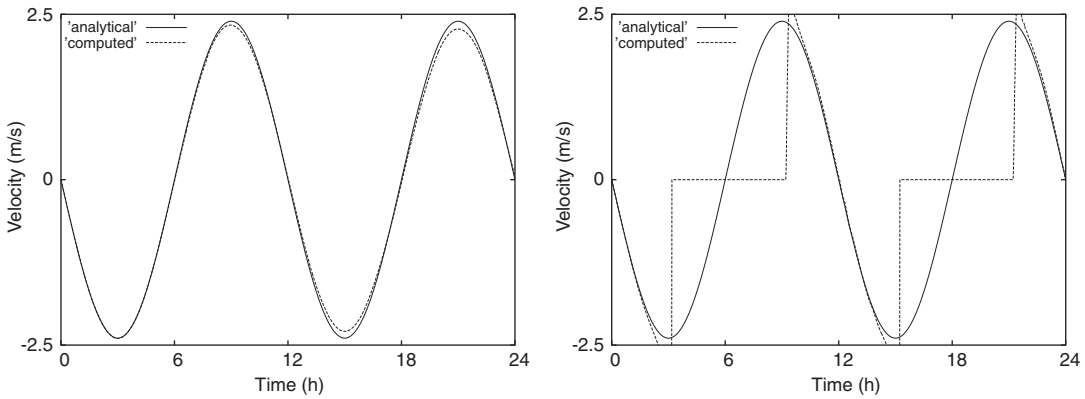

Figure 2. Velocity time series at $x = 100\,\text{km}$ (left) and at $x = L$ (right).

Starting with the initial conditions taken from (16)–(18) with $t = 0$, the numerical solution is computed for two time periods with a time step $\Delta t = 60\,\text{s}$. Figure 2 shows the time series of the computed and the exact values of $U(x, 0, t)$ at $x = 100\,\text{km}$ and $x = L$, respectively. Figure 3 shows the time series of the computed and the exact free-surface elevation $\eta(x, 0, t)$ at $x = 100\,\text{km}$ and L, respectively. The small damping observed in the numerical results is due to the chosen value for the implicitness factor ($\theta = 0.6$) of the model time discretization (see Reference [14] for details).

DOI: 10.1002/fld

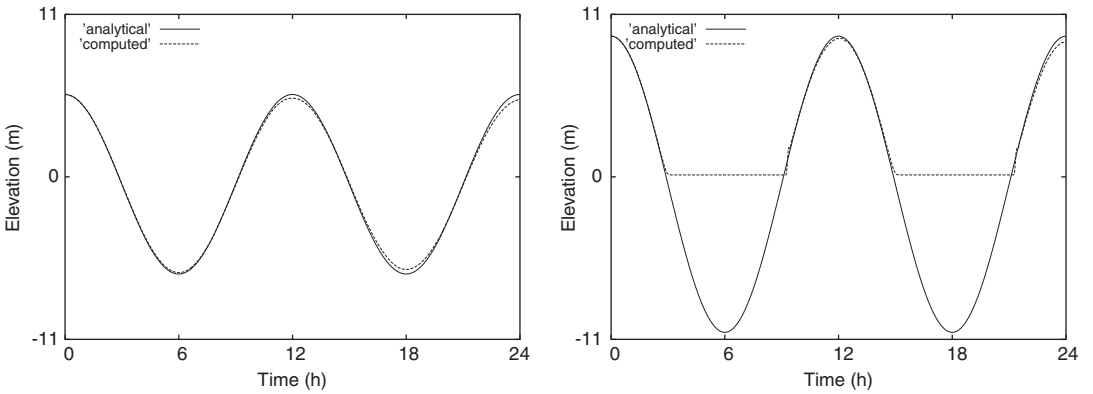

Figure 3. Free-surface elevation time series at $x = 100\,\text{km}$ (left) and at $x = L$ (right).

It is to be noted that, the location $x = L$ becomes dry during half period. Accordingly, during the dry phase the computed velocities and the total water depth at this station are zero simply because the numerical model does not perform any computation in the dry area. Also to be noted is a general good agreement between the analytical and the numerical solutions except at $x = L$ during the transitions from wet to dry and from dry to wet. The numerical error on the computed wet area $A_{\text{wet}} = \pi L^2$ remains below 0.6% during the entire simulation.

These results tend to deteriorate for longer simulations because the stabilizing terms given by bottom friction and horizontal viscosity are not included. Far more difficult to model is the analytical solution corresponding to relatively large values of ψ because of the corresponding larger area that is subject to wetting and drying. In a realistic situation where bottom friction is considered this would have a stabilizing effect especially in the shallowest part of the basin where wetting and drying takes place.

As stated above, since U, V and η as given by (16)–(18) are exact solutions of the two-dimensional equations (11)–(13), then $u = U$, $v = V$ and η are also exact solutions of the three-dimensional equations (1)–(5) with w given by Equation (14) which, in this case, yields

$$w = -uh_x - vh_y = \frac{2h_0}{L^2}\psi\omega(-x\sin\omega t \pm y\cos\omega t) \tag{25}$$

Thus, this analytical solution can be used as a test case for three-dimensional numerical models.

Note that in this specific example, since u and v are independent from the spatial location, the vertical component of the velocity (25) is independent from the vertical coordinate z but is related to the bottom topography.

4. THREE-DIMENSIONAL FLOW WITH PARABOLIC FREE-SURFACE

In a second test case the basin configuration described by Equation (15) is reconsidered and a nontrivial analytical solution whose free-surface is a parabola of revolution was given in Reference [16] for the two-dimensional shallow water Equations (11)–(13). This solution, here

DOI: 10.1002/fld

extended to the three-dimensional equations (1)–(5), is given by

$$u = \frac{1}{2(1 - A\cos\omega t)}\left[\omega x A \sin\omega t - fy\left(\sqrt{1 - A^2} + A\cos\omega t - 1\right)\right] \tag{26}$$

$$v = \frac{1}{2(1 - A\cos\omega t)}\left[\omega y A \sin\omega t + fx\left(\sqrt{1 - A^2} + A\cos\omega t - 1\right)\right] \tag{27}$$

$$w = \frac{\omega A \sin\omega t}{1 - A\cos\omega t}\left(2h_0\frac{x^2 + y^2}{L^2} - h_0 - z\right) \tag{28}$$

$$\eta = h_0\left\{\frac{\sqrt{1 - A^2}}{1 - A\cos\omega t} - 1 - \frac{x^2 + y^2}{L^2}\left[\frac{1 - A^2}{(1 - A\cos\omega t)^2} - 1\right]\right\} \tag{29}$$

where, by setting $\eta_0 = \eta(0, 0, 0)$, the constant A is given by

$$A = \frac{(h_0 + \eta_0)^2 - h_0^2}{(h_0 + \eta_0)^2 + h_0^2} \tag{30}$$

and, for given $\omega > f$, L is given by

$$L = \sqrt{\frac{8gh_0}{\omega^2 - f^2}} \tag{31}$$

The horizontal velocity field (26)–(27) and the free-surface elevation (29) are exactly the same as derived by Thacker for the two-dimensional shallow water equations (see Reference [16] for a detailed derivation). Then, as above, u, v and η are extended to the three-dimensional equations (1)–(5) while the vertical velocity component (28) is derived from Equation (14). An *a posteriori* verification that (26)–(29) is indeed an exact solution of Equations (1)–(5) can be obtained upon direct substitution of (26)–(29) into (1)–(5).

From (26)–(29), this exact solution can be written in polar coordinates (r, ϑ) as

$$u_r = \frac{\omega r A \sin\omega t}{2(1 - A\cos\omega t)} \tag{32}$$

$$u_\vartheta = \frac{fr}{2(1 - A\cos\omega t)}\left(\sqrt{1 - A^2} + A\cos\omega t - 1\right) \tag{33}$$

$$w = \frac{\omega A \sin\omega t}{1 - A\cos\omega t}\left(2h_0\frac{r^2}{L^2} - h_0 - z\right) \tag{34}$$

$$\eta = h_0\left\{\frac{\sqrt{1 - A^2}}{1 - A\cos\omega t} - 1 - \frac{r^2}{L^2}\left[\frac{1 - A^2}{(1 - A\cos\omega t)^2} - 1\right]\right\} \tag{35}$$

Equations (32)–(33) show that the radial component of the velocity u_r is independent of the Coriolis acceleration while the tangential component u_ϑ is proportional to f.

DOI: 10.1002/fld

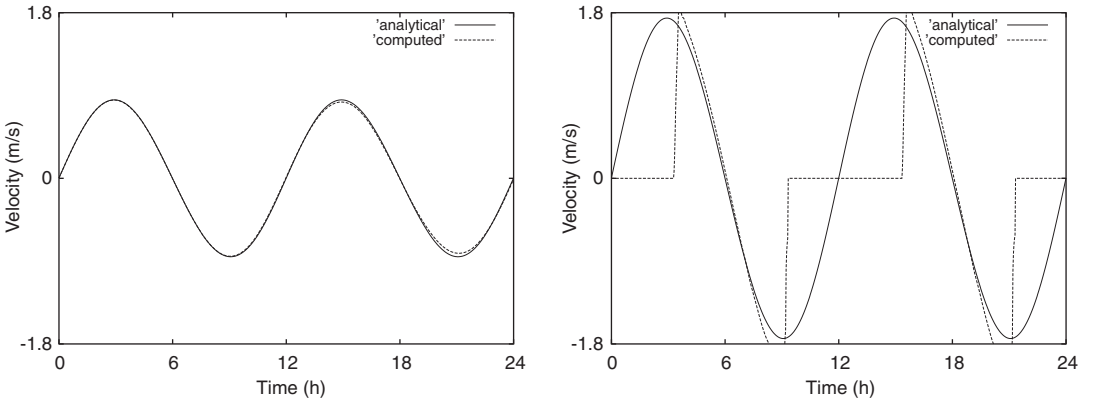

Figure 4. Time series of u_r at $r = 300\,\text{km}$ (left) and at $r = L$ (right).

The shoreline is a circle whose centre coincides with the centre of the basin and the time dependent radius R is given by

$$R^2 = L^2 \frac{1 - A\cos\omega t}{\sqrt{1 - A^2}} \tag{36}$$

Thus, the permanently wet area is confined within the disk $r^2 < L^2[(1 - A)/\sqrt{1 - A^2}]$ and the wetting and drying takes place within the ring $L^2[(1 - A)/\sqrt{1 - A^2}] \leqslant r^2 < L^2[(1 + A)/\sqrt{1 - A^2}]$.

The analytical solution (26)–(29) is defined and satisfies the three-dimensional shallow water Equations (1)–(5) in the entire (x, y, z) space but these equations are of interest only in the wet region where $H > 0$, that is, inside the circle $x^2 + y^2 = R^2$ and for $-h(x, y) < z < \eta(x, y, t)$.

Clearly the exact solution (26)–(29), as well as the corresponding wet area delimited by (36), is strongly influenced by the chosen bottom topography (15) through the constants h_0 and L.

The free parameters h_0, f, ω and η_0 can be chosen in a variety of ways and some realistic values corresponding to a typical environmental flow will be considered. Thus, by setting $h_0 = 50\,\text{m}$, $\eta_0 = 2\,\text{m}$, a latitude of 45°North and $\omega = 2\pi/(12 \times 3600)$, the resulting wave period is $T = 12\,\text{h}$ and from Equation (31) one has $L = 610\,\text{km}$.

An unstructured orthogonal grid is constructed as before by taking mixed, triangular and quadrilateral polygons in such a fashion that their vertices all lie on concentric circles equally spaced at a distance ΔR_1 to cover the permanently wet area (see Figure 1) and a finer mesh obtained by using $\Delta R_2 < \Delta R_1$ to cover the outer ring where wetting and drying takes place. The vertical z-coordinate is discretized with 10 layers separated by constant level surfaces located at $z_{k+1/2} = 5k - 50,\ k = 1, 2, \ldots, 9$.

Starting with the initial conditions taken from (26), (27) and (29) with $t = 0$, the numerical solution is computed for two time periods with a time step $\Delta t = 100\,\text{s}$. The numerical model used is again the semi-implicit algorithm described in Reference [7].

Figure 4 shows the time series of the computed and the exact values of u_r at $r = 300\,\text{km}$ and L, respectively. At the same spatial locations the time series of u_ϑ and η are shown in Figures 5 and 6, respectively. It is to be noted that, the location $r = L$ becomes dry during half period. Accordingly, during the dry phase the computed velocities and the total water depth at this station are zero.

DOI: 10.1002/fld

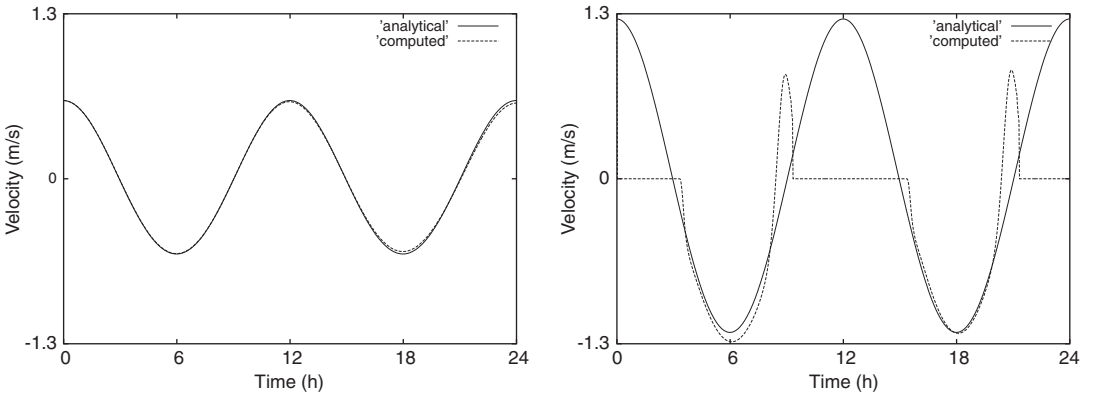

Figure 5. Time series of u_ϑ at $r = 300\,\text{km}$ (left) and at $r = L$ (right).

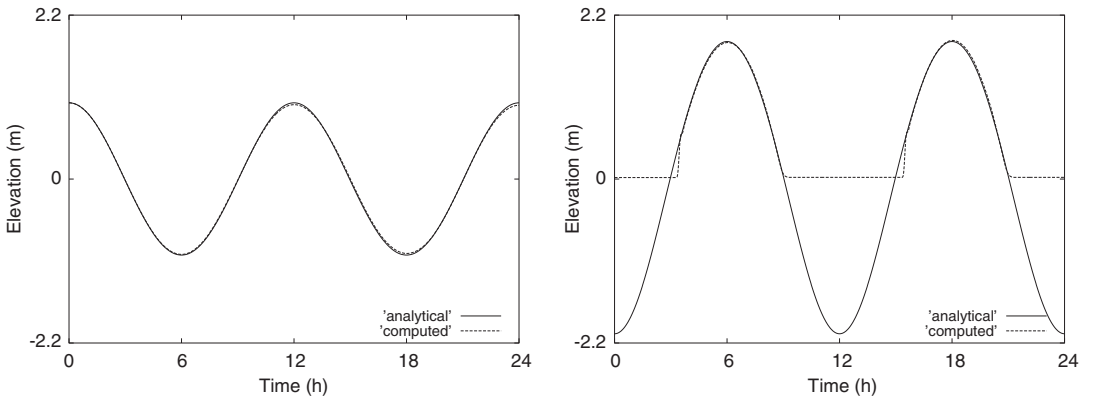

Figure 6. Free-surface elevation time series at $r = 300\,\text{km}$ (left) and at $r = L$ (right).

Figure 7 shows the time series of the computed and the exact values of $w(r, 0, -5, t)$ at $r = 300\,\text{km}$. There is no vertical component of the velocity computed at $r = L$ because, with the present vertical discretization, only one layer is present at $r = L$.

It is worth noting a general good agreement between the analytical and the numerical solutions except at $r = L$ during the transitions from wet to dry and from dry to wet. The relatively high values for u_ϑ are due to the Coriolis forcing at this large scale. Also, the resulting small size of the vertical component of the velocity is due to the relatively large size of the horizontal domain. Though small, accurate determination of the vertical component of the velocity may be extremely important when it is to be used to compute scalar transport that determine fluid stratification. This, however, may not be easy because in hydrostatic models w is diagnostically determined from u and v by using the discrete incompressibility condition. Thus, any numerical error in u and v will unavoidably be reflected in the accuracy of w.

Finally, Figure 8 shows the computed fraction of the wet area. A slight phase shift of the computed results can be observed.

DOI: 10.1002/fld

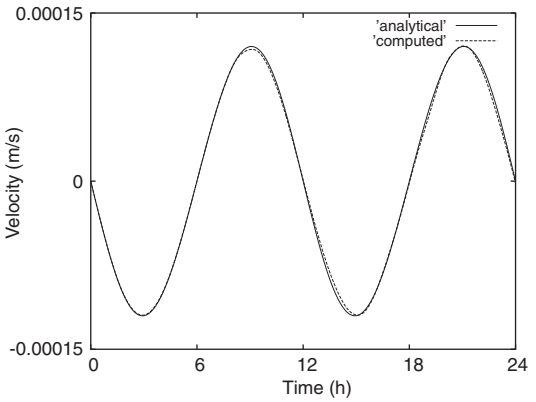

Figure 7. Time series of w at $r = 300\,\text{km}$.

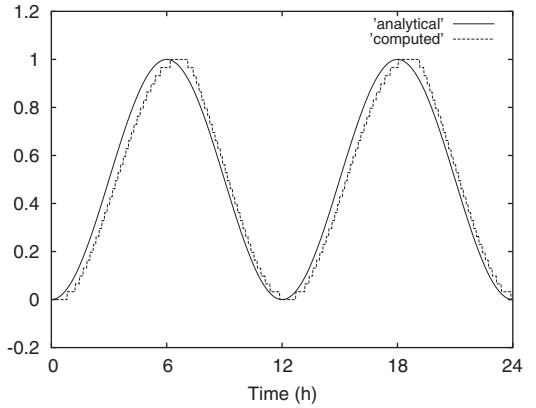

Figure 8. Wet area time series.

The numerical solution would deteriorate in longer simulation because the stabilizing terms given by bottom friction and horizontal viscosity are not included. Far more difficult to model are the analytical solutions corresponding to relatively large values of η_0 because of the resulting larger area that is subject to wetting and drying. In a realistic situation where bottom friction is considered this would have a stabilizing effect especially in the shallowest part of the basin where wetting and drying takes place.

The above example is reconsidered in a much smaller time and horizontal scale. Specifically, h_0, η_0 and f have not been changed but a higher frequency $\omega = 2\pi/12$ is imposed so that the wave period is now $T = 12\,\text{s}$. Equation (31) then yields $L = 120\,\text{m}$. The previous unstructured orthogonal grid has been resized accordingly.

Starting with the initial conditions taken from (26)–(29) with $t = 0$, the numerical solution is computed for two time periods with a smaller time step $\Delta t = 0.028\,\text{s}$. The numerical accuracy

DOI: 10.1002/fld

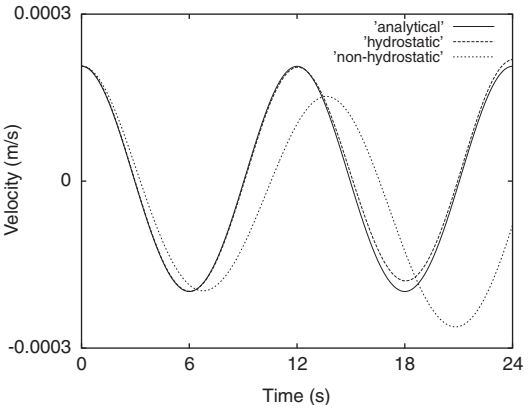

Figure 9. Time series of u_ϑ.

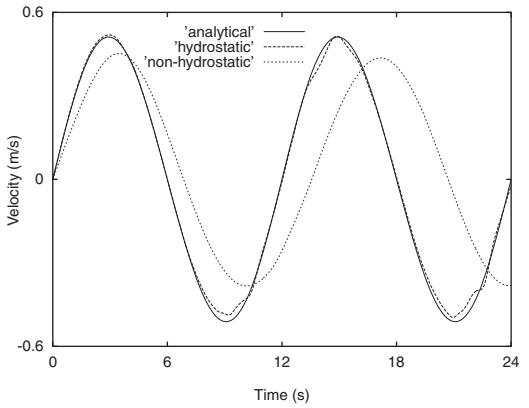

Figure 10. Time series of w.

obtained in this test is qualitatively the same as in the previous example. Figure 9 shows the time series of the computed and the exact tangential horizontal velocity $u_\vartheta(60, 0, -5, t)$ and Figure 10 shows the time series of the vertical component of the velocity at the same location. It is to be noted the good agreement between the exact and the numerical solution. Moreover, at this small scale, the tangential velocity component resulting from the Coriolis forcing term is, as expected, much smaller whereas the vertical component of the velocity is now much larger than the one of the previous example.

As final simulations, these three-dimensional problems have been reconsidered with identical grids, initial conditions and flow parameters but using a more general nonhydrostatic model described in Reference [15]. With no surprise the computed results obtained in the large scale are almost identical to the early hydrostatic results already displayed in Figures 4–8. This is a clear indication that the hydrostatic approximation that lead to the governing equations (1)–(3) is valid at this scale.

DOI: 10.1002/fld

A similar nonhydrostatic simulation performed on the last example with smaller horizontal scale, however, produced totally different results as shown (with dotted lines) in Figures 9 and 10. These results indicate that, although hydrostatic calculations are in good agreement with the corresponding analytical solution, this solution is physically incorrect because the hydrostatic approximation does not apply in such a small horizontal scale. This example confirms that in small scale problems the Coriolis acceleration is usually negligible while the nonhydrostatic pressure term now plays a crucial role (see References [15, 20] for further details).

5. CONCLUSIONS

Some nontrivial analytical solutions of the inviscid, two-dimensional shallow water equations have been extended to three dimension and are proposed as test cases for three-dimensional numerical models. Advective, pressure, and Coriolis acceleration are the only forcing terms for these tests. The tests are further complicated by the wetting and drying nature of the problems. Appropriate choice of the free parameters can give different importance to each driving force which can be tested individually.

These test problems are considered to be quite effective and severe for any numerical model because the often stabilizing contribution of viscosity and bottom friction are not included. A specific semi-implicit numerical scheme is applied in both, the two and the three-dimensional formulations and the computed solution is compared with the exact counterpart. Some examples are illustrated to show how accurate the velocity field and water surface elevation can be reproduced.

It has been verified that, in large horizontal scale, these results can also be reproduced with similar accuracy and negligible differences by using a slower, nonhydrostatic Navier–Stokes model. This confirms that the hydrostatic approximation is valid and computationally convenient at this scale.

It is finally shown that an accurate reconstruction of the analytical solution of the three-dimensional hydrostatic models (1)–(5) can be produced also in relatively small horizontal scale. This solution, however, is physically incorrect because the hydrostatic approximation does not apply to small horizontal scales where physical processes are better described by the Navier–Stokes equations.

REFERENCES

1. Casulli V. Semi-implicit finite difference methods for the two-dimensional shallow water equations. *Journal of Computational Physics* 1990; **86**:56–74.
2. Stelling GS. On the construction of computational methods for shallow water flow problems. *Rijkswaterstaat Communications* 1984; **35**.
3. Walters RA, Casulli V. A robust, finite element model for hydrostatic surface water flows. *Communications in Numerical Methods in Engineering* 1998; **14**:931–940.
4. Hanert E, Legat V, Deleersnijder E. A comparison of three finite elements to solve the linear shallow water equations. *Ocean Modelling* 2003; **5**:17–35.
5. Hanert E, Le Roux DY, Legat V, Deleersnijder E. An efficient Eulerian finite element method for the shallow water equations. *Ocean Modelling* 2005; **10**:115–136.
6. Walters RA. Coastal ocean models: two useful finite element methods. *Continental Shelf Research* 2005; **25**: 775–793.
7. Casulli V, Walters RA. An unstructured grid, three-dimensional model based on the shallow water equations. *International Journal for Numerical Methods in Fluids* 2000; **32**:331–348.

DOI: 10.1002/fld

8. Casulli V, Zanolli P. High resolution methods for multidimensional advection-diffusion problems in free-surface hydrodynamics. *Ocean Modelling* 2005; **10**:137–151.
9. Ham DA, Pietrzak J, Stelling GS. A scalable unstructured grid 3-dimensional finite volume model for the shallow water equations. *Ocean Modelling* 2005; **10**:153–169.
10. Toro EF. *Shock-Capturing Methods for Free-Surface Shallow Flows*. Wiley: New York, 2001.
11. Blumberg AF, Mellor GL. A description of a three dimensional coastal ocean circulation model. In *Three Dimensional Coastal Ocean Circulation Models*, *Coastal and Estuarine Sciences*, Heaps NS (ed.), vol. 4. AGU: Washington, DC, 1987; 1–16.
12. Oey LY. A wetting and drying scheme for POM. *Ocean Modelling* 2005; **9**:133–150.
13. Casulli V, Cheng RT. Semi-implicit finite difference methods for three-dimensional shallow water flow. *International Journal for Numerical Methods in Fluids* 1992; **15**:629–648.
14. Casulli V, Cattani E. Stability, accuracy and efficiency of a semi-implicit method for three-dimensional shallow water flow. *Computers and Mathematics with Applications* 1994; **27**:99–112.
15. Casulli V, Zanolli P. Semi-implicit numerical modeling of non-hydrostatic free-surface flows for environmental problems. *Mathematical and Computer Modelling* 2002; **36**:1131–1149.
16. Thacker WC. Some exact solutions to the nonlinear shallow water equations. *Journal of Fluid Mechanics* 1981; **107**:499–508.
17. Balzano A. Evaluation of methods for numerical simulation of wetting and drying in shallow water flow models. *Coastal Engineering* 1998; **34**:83–107.
18. Lynett PJ, Wu T-R, Liu PL-F. Modeling wave runup with depth-integrated equations. *Coastal Engineering* 2002; **46**:89–107.
19. Hubbard ME, Dodd N. A 2D numerical model of wave run-up and overtopping. *Coastal Engineering* 2002; **47**:1–26.
20. Casulli V, Stelling GS. Numerical simulation of 3D quasi-hydrostatic, free-surface flows. *Journal of Hydraulic Engineering* (ASCE) 1998; **124**:678–686.

DOI: 10.1002/fld